

The open cluster NGC6823 and possible triggered star formation associated with SNR G59.5+0.1

Jin-Long Xu^{1,2,3} and Jun-Jie Wang^{1,3}

¹ National Astronomical Observatories, Chinese Academy of Sciences, Beijing 100012, China

e-mail: xujl@bao.ac.cn

² Graduate University of the Chinese Academy of Sciences, Beijing, 100080, China

³ NAOC-TU Joint Center for Astrophysics, Lhasa 850000, China

Preprint online version: June 17, 2021

ABSTRACT

Aims. We investigate the environment in the vicinity of the supernova remnant (SNR) G59.5+0.1 and identify all young stellar objects (YSOs) around the SNR, to derive the physical properties, obtain insight into the star-formation history, and further see whether SNR G59.5+0.1 can trigger star formation in this region.

Methods. We have performed the submillimeter/millimeter observations in CO lines toward the southeast of SNR G59.5+0.1 with the KOSMA 3m Telescope. High integrated CO line intensity ratio $R_{\text{CO}(3-2)/\text{CO}(2-1)}$ is identified as one good signature of SNR-MCs (molecular clouds) interacting system. To investigate the impact of SNR G59.5+0.1 on the process of star formation, we used GLIMPSE I Catalog to select YSOs (including class I and class II sources).

Results. CO emission in an arc-like shape and mid-infrared 8.28 μm emission are well coincident with SNR G59.5+0.1, which has the total mass of $1.1 \times 10^4 M_{\odot}$ and fully cover open cluster NGC 6823. Three molecular clumps were identified in the CO molecular arc, each clump shows the broad line wing emission, indicating that there are three outflows motion. The integrated CO line intensity ratio ($R_{\text{CO}(3-2)/\text{CO}(2-1)}$) for the whole molecular arc is between 0.48 and 1.57. The maximum value is 1.57, which is much higher than previous measurements of individual Galactic MCs. The CO molecular arc has a line intensity ratio gradient. SNR G59.5+0.1 is in adiabatic expansion phase. The age of the SNR is 8.6×10^4 yr. Based on GLIMPSE I Catalog 625 young stellar objects (YSOs) candidates (including 176 class I sources and 449 class II sources) are selected. The timescales for class 0, class I and class II sources are $\leq 10^4$ yr, $\sim 10^5$ yr, and $\sim 10^6$ yr, respectively. The number of YSOs are significantly enhanced in the interacting regions, indicating the presence of some recently formed stars.

Key words. ISM: clouds — ISM: individual (G59.5+0.1) — ISM: molecules — stars: formation — supernova remnants

1. Introduction

Massive star has significant impact on the morphology and chemical evolution of the surrounding Interstellar Medium (ISM) through UV-radiation, stellar winds, and supernova explosion. Stars form from the densest environments in molecular clouds (MCs), often clustered together spatially in groups ranging from a few sources to many thousands. When a supernova explodes near MCs, shock generated by supernova remnant (SNR) may compress some condensed MCs to collapse. On the other hand, the shock can enhance abundances of the different molecular species with respect to quiescent cloud conditions. So the SNR-MCs interaction plays an essential part in the processes of star formation and the evolution of ISM (Reynoso et al. 2001). These associations are established by the detection of OH 1720 MHz masers, the broad emission lines, high ratio of $^{12}\text{CO } J = 2 - 1$ to $J = 1 - 0$ integrated line intensity, γ -ray emission from MCs toward SNR as well as the morphological relation between SNR and MCs, and so on (Frail et al. 1996; Green et al. 1997; Seta et al. 1998; Wilner et al. 1998; Huang & Thaddeus 1986; Byun et al. 2006; Hewitt & Yusef-Zadeh 2009). Jiang et al (2010) summarized the criteria of the SNR-MCs association. In addition, some results from numerical simulation have speculated that star formation can be triggered by the SNR-MCs interaction (Melioli et al. 2006 & Leao et al. 2009). However, only a

few cases about the triggered star formation have been proposed from the observed results (Junkes et al. 1992; Parons et al. 2009; Xu et al. 2011a).

SNR G59.5+0.1, at a distance of 2.1~2.3 kpc (Xu et al. 2005; Billot et al. 2010), is situated in the direction of Vulpecula OB at the position $(l, b) = (59.58, 0.12)$. According to Xu et al. (2005), the age of SNR G59.5+0.1 is ranges from 10^3 to 10^4 years old. Taylor et al. (1992) described this object as a shell-type SNR with nonthermal spectral index ($\alpha < -0.4$) and with a diameter of 15'. They also mentioned that the SNR is possibly associated with the HII region Sh2-86. Billot et al. (2010) found a circular structure centered at the position of the SNR with a diameter of 15', which confirms the value found by Taylor et al. (1992). Furthermore, Billot et al. (2010) noted a high density of YSOs lined up along two arcs at the northern and southern rims of SNR G59.5+0.1, suggesting that the interaction of the expanding shell of SNR G59.5+0.1 and the neutral gas of Sh2-86 could have triggered the formation of young stars in the cluster. NGC6823 is an open cluster located at R.A(J2000)=19^h43^m08^s.4, Dec(J2000)=23°18'00" with a diameter of $\sim 16'$ (Kharchenko et al. 2005). Riaz et al. (2012) suggested that NGC6823 have possibly experienced a recent burst of star formation, which may be caused by a supernova explosion of massive O star. However, they suggested that SNR

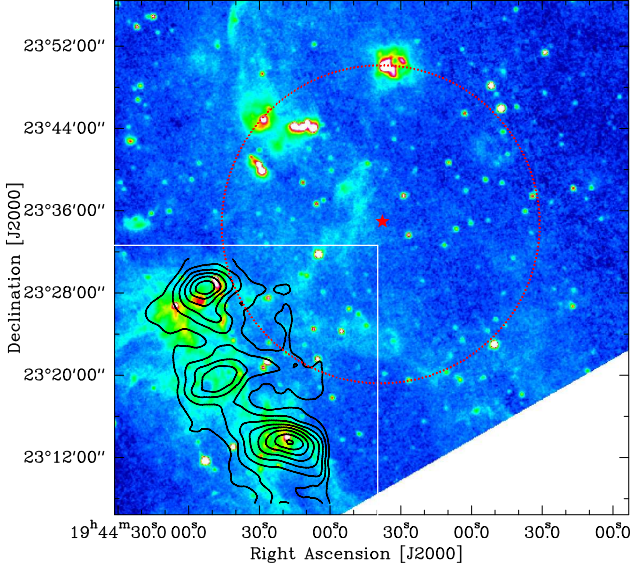


Fig. 1. $^{12}\text{CO } J = 2 - 1$ intensity map (black contours) integrated from 18 to 35 km s^{-1} , overlaid on the the mid-infrared 8.28- μm MSX emission map (color scale). The contour levels are 30, 40, ..., 90% of the peak value (83.9 K km s^{-1}). The red star represents the center of SNR G59.5+0.1 and its extent is outlined by a red dashed circle. The radius of SNR G59.5+0.1 is 15' (Taylor et al. 1992 & Billot et al. 2010). The white box outlines the field seen on the Fig.2.

G59.5+0.1 is not old enough to trigger any of their identified star formation.

Motivated by the supposed association of SNR G59.5+0.1 with molecular gas and with possibly triggered star formation, we have performed $^{12}\text{CO } J = 2 - 1$, $^{12}\text{CO } J = 3 - 2$, and $^{13}\text{CO } J = 3 - 2$ observations toward G59.5+0.1. The observations are described in §2, and the results are presented in §3. In §4, we discuss how our data lend supportive evidence of the triggered star formation in the interacting region. The conclusions are summarized in §5.

2. Observations

The mapping observations of G59.5+0.1 were made in $^{12}\text{CO } J = 2 - 1$, $^{12}\text{CO } J = 3 - 2$ and $^{13}\text{CO } J = 2 - 1$ lines using the KOSMA 3m telescope at Gornergrat, Switzerland, in April 2004. The half-power beam widths of the telescope at the observing frequencies of 230.538 GHz, 345.789 GHz and 220.399 GHz are 130'', 80'', and 130'', respectively. The pointing and tracking accuracy is better than 20''. The accuracy of the absolute intensity calibration to be better than 15% (Sun et al. 2008). The DSB receiver noise temperature was about 170 K. The medium and variable resolution acousto optical spectrometers have 1501 and 1601 channels, with total bandwidth of 248 MHz and 544 MHz. The channel widths of 165 and 340 kHz correspond to velocity resolutions of 0.21 and 0.29 km s^{-1} , respectively. The beam efficiency B_{eff} is 0.68 at 230 GHz and 220 GHz. The beam efficiency B_{eff} is 0.72 at 345 GHz. The forward efficiency F_{eff} is 0.93. Mapping observations are centered at RA(J2000)=19^h43^m47.85^s, DEC(J2000)=23°21'26.34'' using the On-The-Fly mode, the total mapping area is 24'×24' in $^{12}\text{CO } J = 2 - 1$ and $^{12}\text{CO } J = 3 - 2$ with a 1'×1' grid, while the mapping area in $^{13}\text{CO } J = 2 - 1$ is 10'×15'.

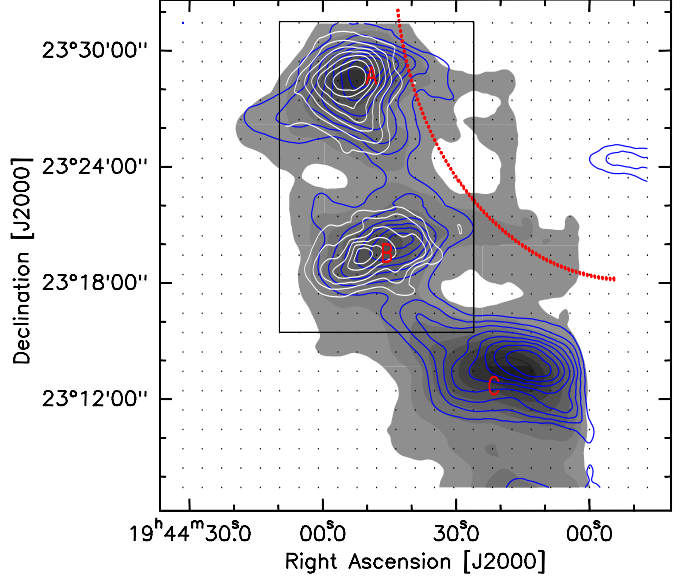


Fig. 2. $^{12}\text{CO } J = 2 - 1$ intensity map (gray scale), overlaid on $^{12}\text{CO } J = 3 - 2$ (blue contours) and $^{13}\text{CO } J = 2 - 1$ (white contours) intensity maps. The contour levels of each CO molecule are 30, 40, ..., 90% of the peak value. The $^{12}\text{CO } J = 3 - 2$ and $^{13}\text{CO } J = 2 - 1$ peak values are 79.0 and 15.5 K km s^{-1} , respectively. Letter A, B and C indicate the different MC clumps. The dot symbols mark the mapping points of $^{12}\text{CO } J = 2 - 1$ and $^{12}\text{CO } J = 3 - 2$, while the black rectangle outlines the mapped field of $^{13}\text{CO } J = 2 - 1$.

The data were reduced using the GILDAS/CLASS¹ package. The correction for the line intensities to the main beam temperature scale was made using the formula $T_{\text{mb}} = (F_{\text{eff}}/B_{\text{eff}} \times T_{\text{A}}^*)$.

3. Results

3.1. Molecular emission

Figure 1 presents the emission map (color scale) at 8.28 μm . The emission shows a half-shell morphology, which is associated with SNR G59.5+0.1 with a diameter of 15'. The integrated intensity map of $^{12}\text{CO } J = 2 - 1$ is overlapped the 8.28 μm emission located in the white boxed area of Figure 1, which covers open cluster NGC6823 marked in a green dashed circle (see Figure 8). The $^{12}\text{CO } J = 2 - 1$ emission coincides well with the 8.28 μm emission at the southeast. In order to further analyze the morphology of CO molecular gas, we make the integrated intensity map of $^{12}\text{CO } J = 3 - 2$ and $^{13}\text{CO } J = 2 - 1$ (Figure 2). In Figure 2, $^{12}\text{CO } J = 2 - 1$ emission is coincident with that from $^{12}\text{CO } J = 3 - 2$ and $^{13}\text{CO } J = 2 - 1$. The $^{12}\text{CO } J = 2 - 1$ and $^{12}\text{CO } J = 3 - 2$ emission appear to show a arc-like structure, while the $^{13}\text{CO } J = 2 - 1$ emission may trace the compact core of molecular gas. We find three cloud clumps in this structure, each clump is designated alphabetically, clump A, clump B and clump C. Because the mapping area in $^{13}\text{CO } J = 2 - 1$ is smaller (see section 2), we did not detected the $^{13}\text{CO } J = 2 - 1$ emission from the clump C. Figure 3 shows $^{12}\text{CO } J = 2 - 1$, $^{12}\text{CO } J = 3 - 2$ and $^{13}\text{CO } J = 2 - 1$ spectra averaged over clump A, clump B and clump C, respectively. Line profiles of $^{12}\text{CO } J = 2 - 1$ and $^{12}\text{CO } J = 3 - 2$ for each clump appear to be broadened, the velocity components are mainly located in interval 18 to 35 km s^{-1} . The

¹ <http://www.iram.fr/IRAMFR/GILDAS/>

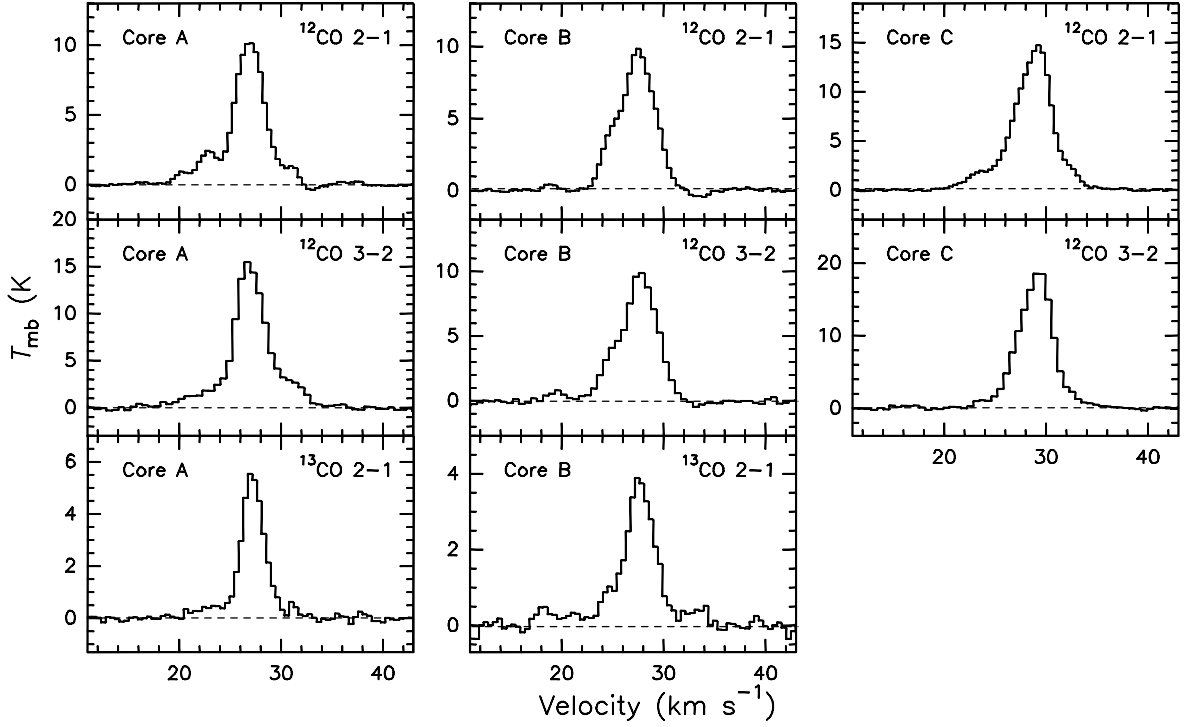


Fig. 3. Averaged spectra of molecular line $^{12}\text{CO } J = 2 - 1$, $^{12}\text{CO } J = 3 - 2$ and $^{13}\text{CO } J = 2 - 1$ over each clump. The dashed lines mark the position at the zero intensity.

Table 1. Observed parameters of each line

Name	$^{12}\text{CO } 2-1$			$^{12}\text{CO } 3-2$			$^{13}\text{CO } 2-1$		
	T_{mb} (K)	FWHM (km s^{-1})	V_{LSR} (km s^{-1})	T_{mb} (K)	FWHM (km s^{-1})	V_{LSR} (km s^{-1})	T_{mb} (K)	FWHM (km s^{-1})	V_{LSR} (km s^{-1})
Core A	9.9 (0.6)	3.7 (0.2)	27.0 (0.1)	14.5 (0.4)	3.9(0.1)	27.0 (0.1)	5.4 (0.2)	2.7 (0.1)	27.3 (0.1)
Core B	9.2 (0.2)	4.4 (0.1)	27.4 (0.1)	9.4 (0.2)	4.4(0.1)	27.6 (0.1)	3.6 (0.2)	3.6 (0.2)	27.6 (0.2)
Core C	13.9 (0.3)	4.4 (0.1)	28.8 (0.1)	18.3 (0.3)	4.0(0.1)	29.0 (0.1)	—	—	—

Note: The position of clump A is at RA(J2000)= $19^{\text{h}}43^{\text{m}}51.85^{\text{s}}$ and DEC(J2000)= $23^{\circ}28'26.34''$; The position of clump B is at RA(J2000)= $19^{\text{h}}43^{\text{m}}47.85^{\text{s}}$ and DEC(J2000)= $23^{\circ}19'26.34''$; The position of clump C is at RA(J2000)= $19^{\text{h}}43^{\text{m}}15.85^{\text{s}}$ and DEC(J2000)= $23^{\circ}13'26.34''$.

spectral profile of clump A may show a broad outflow wing and has two weaker components at 23 km s^{-1} and 31 km s^{-1} . We have made Gaussian fits to all the spectra. The fitted results are summarized in Table 1. From Table 1, we derive systemic velocities of $\sim 27.1 \text{ km s}^{-1}$, $\sim 27.5 \text{ km s}^{-1}$, and $\sim 28.9 \text{ km s}^{-1}$ in clump A, clump B, and clump C, respectively. According to the galactic rotation model of Fich et al. (1989) together with $R_{\odot} = 8.5 \text{ kpc}$ and $V_{\odot} = 220 \text{ km s}^{-1}$, where V_{\odot} is the circular rotation speed of the Galaxy, we obtain a kinematic of 2.3 kpc for the distance of all clumps, which is roughly consistent with the photometric distance ($2.1 \pm 0.1 \text{ kpc}$) of NGC 6823 (Guetter 1992).

Assuming local thermodynamical equilibrium (LTE) and using the $^{12}\text{CO } J = 2 - 1$ line, the column density of the clumps in cm^{-2} is estimated as (Garden et al. 1991; Xu et al. 2010)

$$N_{\text{clu}} = 1.08 \times 10^{13} \frac{(T_{\text{ex}} + 0.92)}{\exp(-16.62/T_{\text{ex}})} \int T_{\text{mb}} \times \frac{\tau dv}{[1 - \exp(-\tau)]}, \quad (1)$$

where dv is the velocity range in km s^{-1} , T_{ex} is the excitation temperature in K, and τ is the optical depth for $^{12}\text{CO } J = 2 - 1$ line. T_{ex} is estimated following the equation $T_{\text{ex}} =$

$11.1/\ln[1 + 1/(T_{\text{mb}}/11.1 + 0.02)]$, while we calculate τ according to

$$\frac{T_{\text{mb}}(^{12}\text{CO})}{T_{\text{mb}}(^{13}\text{CO})} \approx \frac{1 - \exp(-\tau)}{1 - \exp(-\tau/89)}, \quad (2)$$

where T_{mb} is the corrected main beam temperature. Here we assume the solar abundance ratio of $[^{12}\text{CO}]/[^{13}\text{CO}]=89$ (Lang 1980; Anders & Grevesse 1989; Garden et al. 1991), and that the $^{12}\text{CO } J = 2 - 1$ emission is optically thick. Additionally, we use the relation $N_{\text{H}_2} \approx 10^4 N_{^{12}\text{CO}}$ (Dickman 1978). If the clumps are approximately spherical in shape, the mean number density H_2 is $n(\text{H}_2)=1.62 \times 10^{-19} N_{\text{H}_2}/L$, where L is the clump diameter in parsecs (pc). Furthermore, their mass is given by $M_{\text{H}_2}=n(\text{H}_2)\frac{1}{6}\pi L^3 \mu_g m(\text{H}_2)$ (Garden et al. 1991), where $\mu_g=1.36$ is the mean atomic weight of the gas, and $m(\text{H}_2)$ is the mass of a hydrogen molecule. The derived column density, mean number density, and mass of each clump may be in error by as much as a factor of three depending on the exact value of the $[^{12}\text{CO}]/[^{13}\text{CO}]$ abundance ratio (Garden et al. 1991), which are all listed in Table 2.

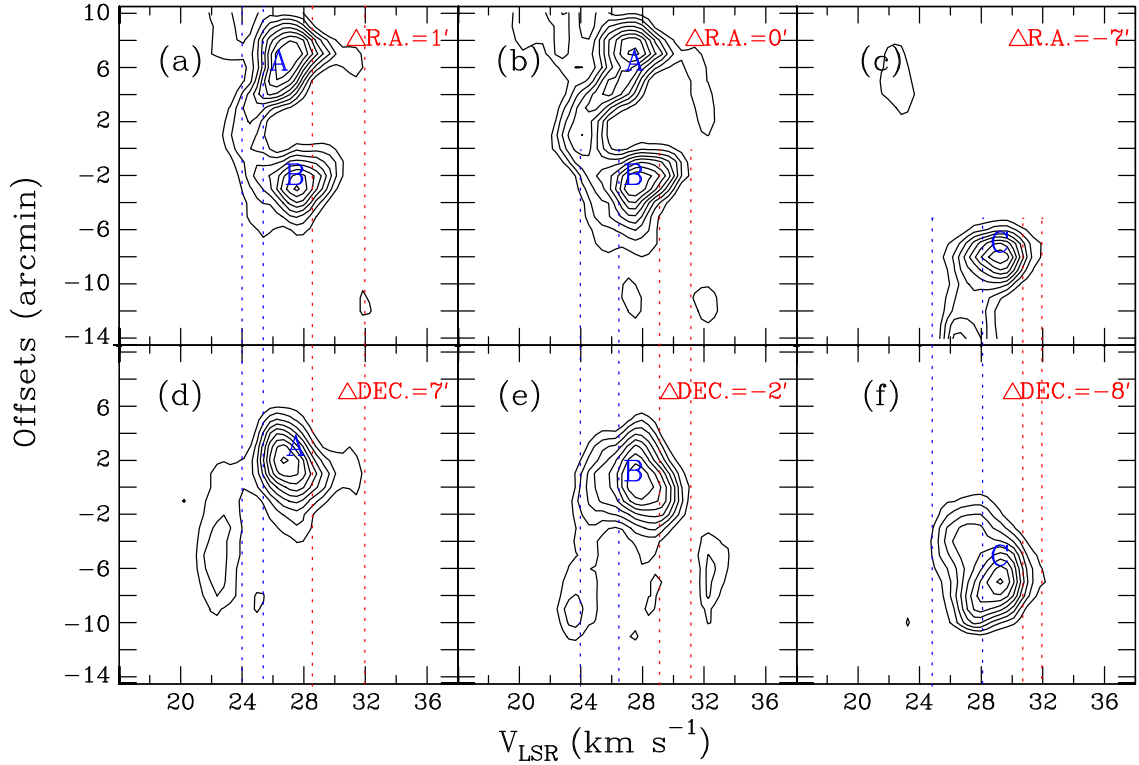


Fig. 4. P-V diagram constructed from CO $J = 2 - 1$ transition for clump A-C. (a)-(c) panels: Contour levels are 10, 20,..., 90% of the peak value, with a cut through the peak positions of each clump along the north-south direction, the peak positions are shown in the upper right corner. (d)-(f) panels: Contour levels are the same as above panels, with a cut along the east-west direction. The blue and red vertical dashed lines mark the velocity ranges of the blueshifted and redshifted emission for each clump, respectively. The offsets given in each panel are relative to RA(J2000)=19^h43^m47.85^s and DEC(J2000)=23°21'26.34".

Table 2. The physical parameters of the clumps in LTE.

Name	T_{ex} K	L pc	N_{H_2} (cm^{-2})	$n(\text{H}_2)$ (cm^{-3})	M ($10^3 M_{\odot}$)
Clump A	15.0	5.4	1.4×10^{22}	4.2×10^2	6.3
Clump B	14.3	4.7	0.9×10^{22}	3.3×10^2	3.2
Clump C	19.2	6.3	2.2×10^{22}	5.6×10^2	1.4

To determine the velocity components and confirm the outflow, we have made position-velocity (PV) diagrams with the cuts through the peak positions of each clump along the north-south and east-west directions, as shown in Figure 4. From Figure 4, we can clearly identify three clumps. Each clump shows the bipolar structure marked by the blue and red vertical dashed lines. The blueshifted and redshifted components have obvious velocity gradients, in particular for clump A and clump B presented in panel (d) and (e) of Figure 4. The distributions of redshifted and blueshifted velocity components are a indication of outflow motion. In panel (d), we also identify a velocity component from 21 to 24 km s^{-1} , which is not from the component of the outflow, but related to a $^{12}\text{CO } J = 2 - 1$ weaker component peaked at -23 km s^{-1} as seen from the $^{12}\text{CO } J = 2 - 1$ spectra of clump A in Figure 3. Using the velocity ranges obtained from the PV diagram, we made the velocity integrated intensity maps superimposed on each clump emission map, respectively. The distribution of redshifted and blueshifted velocity components in Figure 5 provides us further evidence for the bipolar outflow in each clump.

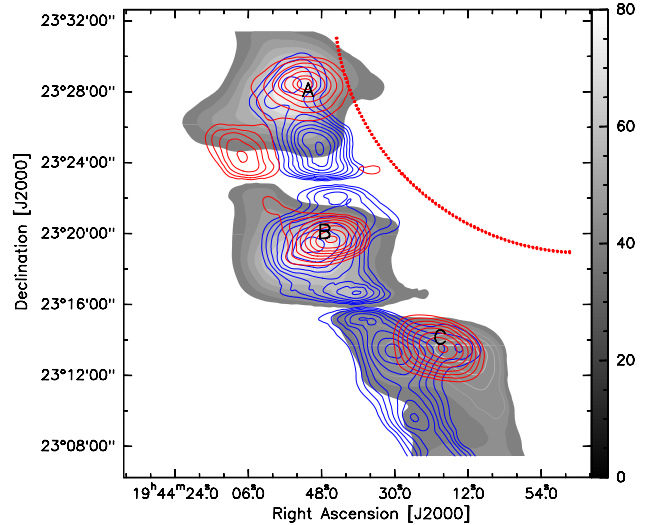


Fig. 5. The velocity integrated intensity maps of $^{12}\text{CO } J = 2 - 1$ outflows (red and blue contours) overlaid with the $^{12}\text{CO } J = 2 - 1$ emission of each clump (gray scale). The red and blue contour levels are 20, 30,...,100% of the peak value. The red dashed arc represents SNR G59.5+0.1.

When a supernova expands into the surrounding molecular clouds, the shocks resulting from the interaction of SNR with MCs can heat the surrounding gases. As the temperature of gases increases, the line opacities decrease as the upper J levels become more populated, then the integrated intensity ratio of ^{12}CO

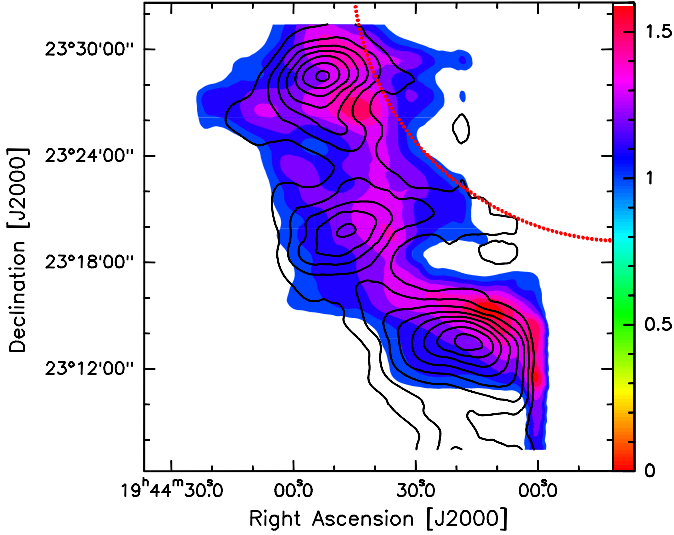


Fig. 6. $^{12}\text{CO } J = 2 - 1$ intensity map are superimposed on the line intensity ratio map (color scale), the line intensity ratios ($R_{I_{\text{CO}(3-2)}/I_{\text{CO}(2-1)}}$) range from 0.48 to 1.57 by 0.16. The wedge indicates the line intensity ratios scale.

$J = 3 - 2$ to $^{12}\text{CO } J = 2 - 1$ ($R_{I_{\text{CO}(3-2)}/I_{\text{CO}(2-1)}}$) can indicate the shock (Xu et al. 2011a; 2011b). In order to obtain the integrated intensity ratio of $^{12}\text{CO } J = 3 - 2$ to $^{12}\text{CO } J = 2 - 1$, the $80''$ resolution of $^{12}\text{CO } J = 3 - 2$ data is convolved with an effective beam size of $\sqrt{130^2 - 80^2} = 102''$. We calculated the integrated intensities for $^{12}\text{CO } J = 3 - 2$ line in the same velocity range as for $^{12}\text{CO } J = 2 - 1$ line. The integrated range is from 16 to 36 km s^{-1} . Figure 6 shows the distribution of $R_{I_{\text{CO}(3-2)}/I_{\text{CO}(2-1)}}$ (color scale) overlaid with the distribution of $^{12}\text{CO } J = 2 - 1$ line integrated intensity (contours). The red dashed arc represents SNR G59.5+0.1. In Figure 6, the whole arc-like molecular gas has a ratio value gradient increasing from northeast to southwest, suggesting that SNR shock is expanding into clump A-C and start to compress each clump. The ratio values for the clump A, clump B, and clump C are between 0.48 and 1.57. The maximum value is 1.57, which is much higher than typical value (0.55) for MCs in the Galactic disk (Sanders et al. 1993) and value (0.69) for the normal MCs in M33 (0.69 Wilson et al. 1997), and even higher than value (0.8) in the starburst galaxies M82 (Gusten et al. 1993).

3.2. Infrared emission

To further search for primary tracers of the star-formation activity in the surrounding of G59.5+0.1, we used the GLIMPSE I Catalog which consists of point sources that are detected at least twice in one band. The GLIMPSE I survey observed the Galactic plane ($65^\circ < |l| < 10^\circ$ for $|b| < 1^\circ$) with the four mid-IR bands (3.6, 4.5, 5.8, and $8.0 \mu\text{m}$) of the Infrared Array Camera (IRAC; Fazio et al. 2004) on the Spitzer Space Telescope. From the database, we selected 29469 near-infrared sources within a circle of $24'$ in radius centered on R.A.= $19^{\text{h}}42^{\text{m}}50^{\text{s}}$ (J2000), Dec= $+23^\circ30'00''$ (J2000). The size of this region completely covers the extension of G59.5+0.1 and the open cluster NGC6823. Figure 7 shows the $[5.8] - [8.0]$ versus $[3.6] - [4.5]$ color-color (CC) diagram. The regions in the figure indicate the stellar evolutionary stages based on the criteria of Allen et al. (2004), Parons et al (2009), and Petriella et al (2010a). The near-infrared sources are classified into three regions: class I

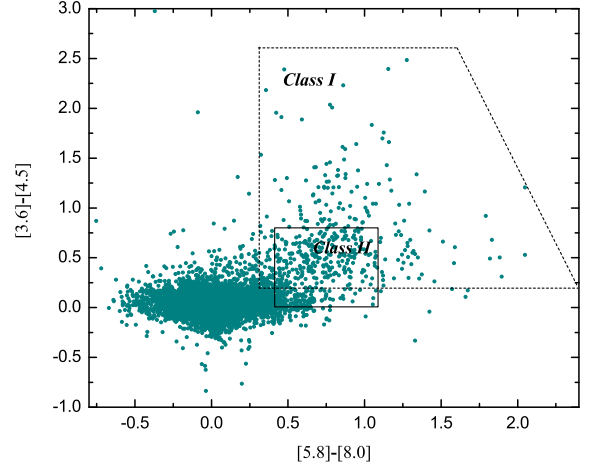


Fig. 7. GLIMPSE color-color diagram $[5.8] - [8.0]$ versus $[3.6] - [4.5]$ for sources. The regions indicate the stellar evolutionary stage as defined by Allen et al. (2004). Class I sources are protostar with circumstellar envelopes and class II are disk dominated objects.

sources are protostars with circumstellar envelopes (polygon), class II sources are disk-dominated objects (rectangle), and other sources. Using this criteria, we find 176 class I sources and 449 class II sources. Here class I and class II sources are chosen to be YSOs.

Figure 8 shows the spatial distribution of both class I and class II sources. From Figure 8, we note that class I and class II sources are not symmetrically distributed in the whole selected region, and are mostly concentrated in the north and southeast around SNR G59.5+0.1, which is similar to the results of Billot et al. (2010). Regarding the geometric distribution of class I and class II sources, we can plot the map of the star surface density. Because class I sources is younger than class II sources and the spatial distribution of class II sources is similar to that for class I sources, we only plot the map of the star surface density for class I sources. This map was obtained by counting all class I sources with a detection in the $3.6 \mu\text{m}$, $4.5 \mu\text{m}$, $5.8 \mu\text{m}$, and $8.0 \mu\text{m}$ bands in squares of $4' \times 4'$, as shown in Figure 9. From Figure 9 we can see that there are clear signs of clustering toward the region where SNR G59.5+0.1 is close approximately to the surrounding ISM. The existence of class I sources may also indicate star formation activity.

4. Discussion

4.1. SNR G59.5+0.1 and MCs

Because of the high confusion level in the surrounding of Sh2-86 structured emission, both Reach et al. (2006) and Billot et al. (2010) did not detect SNR G59.5+0.1. Similarly, we could not detect the SNR on the $8.28 \mu\text{m}$ image, but detected the $8.28 \mu\text{m}$ emission which present the half-shell structure around the SNR. The half-shell emission may be produced by SNR G59.5+0.1 and/or the stellar winds of its progenitor. We have performed the submillimeter/millimeter observations in CO lines toward the southeast of SNR G59.5+0.1. The $^{12}\text{CO } J = 2 - 1$ molecular emission is coincident very well with the $8.28 \mu\text{m}$ emission, which covers the whole size of NGC 6823. In addition, the $^{12}\text{CO } J = 2 - 1$ molecular emission shows the arc-like morphology. We identified three clumps in the molecular arc. Three bipolar outflows are detected in these clumps

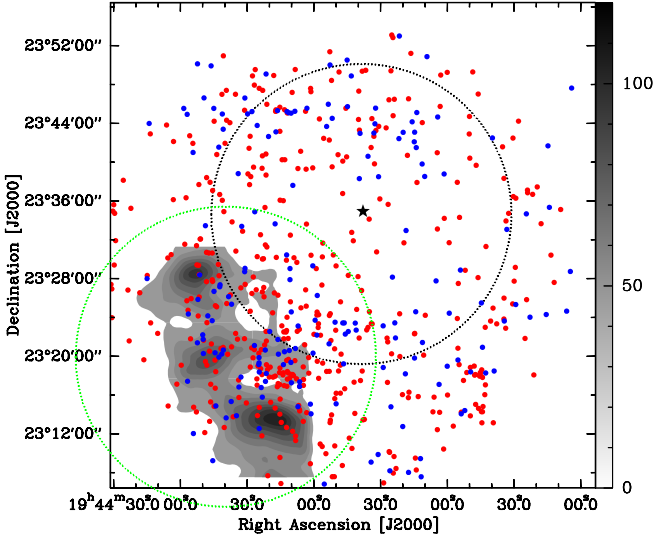


Fig. 8. Positions of Class I and II sources relative to the $^{12}\text{CO } J = 2 - 1$ MCs (grey scale) around SNR G59.5+0.1. The Class I sources are labeled as the blue dots; The Class II sources are labeled as the red dots. The black and green dashed circles represent SNR G59.5+0.1 and open cluster NGC6823, respectively.

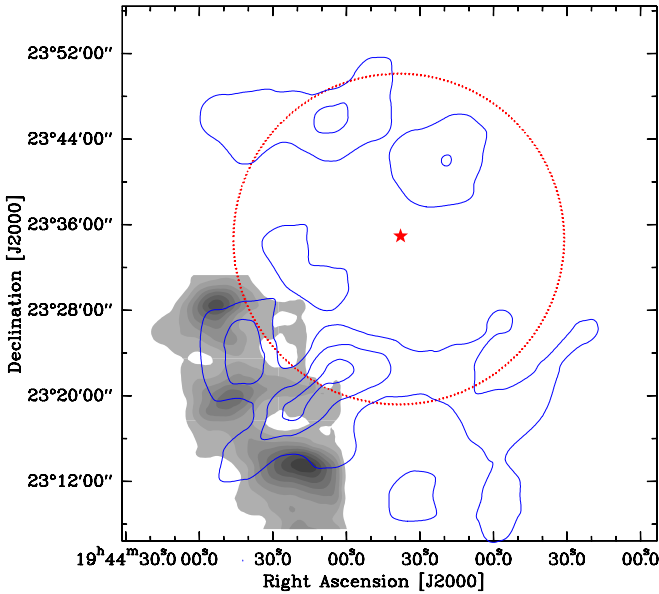


Fig. 9. Stellar-surface density map of Class I candidates are superimposed on $^{12}\text{CO } J = 2 - 1$ MCs (grey scale) around SNR G59.5+0.1. Contours range from 2 to 10 stars $(4\text{arcmin})^{-2}$ in steps of 4 stars $(4\text{arcmin})^{-2}$. 1σ is $0.7 (4\text{arcmin})^{-2}$ (background stars).

around SNR G59.5+0.1 for the first time. The line profile of $^{12}\text{CO } J = 2 - 1$ in clump A appear to be broadened, which may be not only caused by the outflows, but also by shock from SNR G59.5+0.1. The maximum value of $R_{I_{\text{CO}(3-2)}/I_{\text{CO}(2-1)}}$ is 1.6 in the molecular arc, which is higher than that in the previous measurement of individual Galactic MCs. High $R_{I_{\text{CO}(3-2)}/I_{\text{CO}(2-1)}}$ is suggested as a signature of the SNR-MC interaction system (Jiang et al. 2010; Xu et al. 2011a). Together, these observations strongly indicate that the MCs are interacting with G59.5+0.1. SNR G59.5+0.1 just start to interact with the surrounding MCs,

so the MCs have the $R_{I_{\text{CO}(3-2)}/I_{\text{CO}(2-1)}}$ gradient along the shock direction. We suggest that the distribution of $R_{I_{\text{CO}(3-2)}/I_{\text{CO}(2-1)}}$ value is a good signature of the SNR-MCs interaction system. The integrated CO intensity ratios ($R_{I_{\text{CO}(3-2)}/I_{\text{CO}(2-1)}}$) may be used to study other triggering mechanism of star formation, such as the shocks of cloud-cloud collision, HII regions and galactic density waves. From Table 2, the total mass of MCs associated with SNR G59.5+0.1 is $1.1 \times 10^4 M_{\odot}$.

4.2. Recent star formation in the MCs

To summarize the results from investigating the spatial distribution of YSOs, we clearly see that the distribution of YSOs (class I and class II sources) is clustered around the border of SNR G59.5+0.1. The best correlation is found with the CO molecular arc in the southeast where most of YSOs may belong to open cluster NGC6823. It is unlikely that they all are just foreground and background stars. It is more likely that those YSOs are physically associated with the interacting regions between G59.5+0.1 and MCs. Riaz et al. (2012) suggested that NGC6823 have possibly experienced a recent burst of star formation, which may be caused by a supernova explosion of massive O star. Also, these YSOs distribution is clustered together and shows a shell-like structure around G59.5+0.1. SNR G59.5+0.1 is close approximately to NGC6823. We suggest that SNR G59.5+0.1 possibly have triggered these YSOs formation and star formation in this cluster. Class I sources occur in a period on the order of $\sim 10^5$ yr, while the age of class II sources is $\sim 10^6$ yr (André & Montmerle 1994).

In an inhomogeneous medium, an SNR can be undergoing different evolutionary stages in different places at the same time. If an SNR is in radiative expansion phase, the radius of an SNR is ~ 30 pc (Heiles 1964). Here the radius of SNR G59.5+0.1 is ~ 10 pc, the SNR has not yet been achieved the radiative phase, but in adiabatic expansion. The age of G59.5+0.1 given by Sedov equation (Reynoso & Manguerra 2001) in units of 10^4 yr:

$$t_s = (R_s/13.6)^{5/2} \left(\frac{n_0}{E_{51}} \right)^{1/2}. \quad (3)$$

where E_{51} is the remnant energy, we adopt a canonical value of 10^{51} ergs. R_s is the remnant radius, while n_0 is the ambient number density in cm^3 , which is determined by Table 2. Then we obtain that the age of G59.5+0.1 is 8.6×10^4 yr. The age of G59.5+0.1 are shorter than that of these YSOs, which is 10^5 to 10^6 yr. Hence the formation of the YSOs may not be triggered by the shock of SNR G59.5+0.1. Because SNR G54.4-0.3, SNR G24.7+0.6 and SNR IC443 are not old enough, Junkes et al. (1992), Petriella et al. (2011), and Xu et al. (2011a) suggested that the YSOs around the remnants may not be triggered by the remnants, but triggered by the stellar winds of the remnants progenitors. SNR G59.5+0.1 is located in the direction of Vulpecula OB at the position $(l, b) = (59.58, 0.12)$, hence the spectral type of SNR G59.5+0.1 progenitor may be O or B. In the course of high-mass stars evolution the stellar winds go through three phases (Dwarkadas 2007), which last for about 4.6×10^6 yr. Such periods of stellar winds are sufficient to form YSOs. We conclude that the formation of the YSOs may be triggered by the stellar winds from the high-mass progenitor of G59.5+0.1.

Outflow is a strong evidence of the earlier star forming activity. We detected three outflows around SNR G59.5+0.1. The dynamic timescale of each outflow is given by equation $t = 9.78 \times 10^5 R/V$ (yr), where R in pc is the outflow size defined by the average of the radius of the blueshifted and redshifted lobes, V in km s^{-1} is the maximum flow velocity relative to the cloud

systemic velocity. The obtained average dynamical timescales of outflow A-C are $\sim 7.4 \times 10^3$ yr, $\sim 5.3 \times 10^3$ yr, and $\sim 5.2 \times 10^3$ yr, suggesting that there are three Class 0 protostars ($\leq 10^4$ yr). These Class 0 protostars are distributed around SNR G59.5+0.1. SNR G59.5+0.1 with an age of 8.6×10^4 yr may trigger the formation of these Class 0 protostars. The observations with higher spatial resolutions are needed to further analyze these protostars.

5. Conclusions

We have presented the $^{12}\text{CO } J = 2 - 1$, $^{12}\text{CO } J = 3 - 2$, and $^{13}\text{CO } J = 2 - 1$ molecular and infrared observations towards SNR G59.5+0.1. These results can be summarized as follows:

1. The arc-like morphological association with SNR G59.5+0.1, the broadened emission lines, and the high integrated CO line intensity ratio ($R_{I_{\text{CO}(3-2)}/I_{\text{CO}(2-1)}} \sim 1.58$) suggest that these cloud clumps are interacting with G59.5+0.1. The age of the SNR is 8.6×10^4 yr. The whole molecular gas in the southeast have a line intensity ratio gradient along the direction of shock, implying that shocks have driven into cloud clumps. We suggest that high $R_{I_{\text{CO}(3-2)}/I_{\text{CO}(2-1)}}$ is identified as one good signature to study the triggering mechanism of star formation, such as the shocks of cloud-cloud collision, HII regions, and Galactic density waves. The cloud clumps have the total mass of $1.1 \times 10^4 M_{\odot}$.
2. The selected young stellar objects (YSOs) (including class I and class II sources) are concentrated and grouped around the interacting regions. It provides strong signpost for ongoing star formation. Comparing the age of G59.5+0.1 and the timescales of the stellar winds of G59.5+0.1 progenitor with the characteristic star-formation timescales, we conclude that the YSOs may not be triggered by SNR G59.5+0.1, but triggered by the stellar winds of G59.5+0.1 progenitor.
3. Three young outflows are detected in the clumps around SNR G59.5+0.1. It may be the first SNR around which find such more outflows in all the Galaxy SNRs. Taking into account the age of SNR G59.5+0.1 and class 0 source, we find that SNR G59.5+0.1 may trigger the formation of these Class 0 sources. It also may provide us a direct evidence for star formation triggered by SNR. The results of the present work confirm the sequential star formation on the basis of the different ages of star formation associated with SNR G59.5+0.1.

Acknowledgements. We would like to thank Dr. Sheng-Li Qin for his help on data acquirement and discussion. We also thank the anonymous referee for his/her constructive comments and suggestions that greatly improved the content and presentation of this paper. Jin-Long Xu's research is in part supported by 2011 Ministry of Education doctoral academic prize. Supported by the young Researcher Grant of National Astronomical Observations, Chinese Academy of Sciences.

References

Allen, L. E., Calvet, N., D'Alessio, P., 2004, *ApJS*, 154, 363
 André, P., & Montmerle, T., 1994, *ApJ*, 420, 837
 Anders, E., & Grevesse, N. 1989, *Geochim. Cosmochim. Acta*, 53, 197
 Billot, N., Noriega-Crespo, A., Carey, S., Guieu, S., Shenoy, S., Paladini, R., & Latter, W., 2010, *ApJ*, 712, 797
 Byun, D.-Y., Koo, B.-C., Tatematsu, K., Sunada, K. 2006, *ApJ*, 637, 283
 Casoli, F., Combes, F., Dupraz, C., Gerin, M., & Boulanger, F., 1986, *A&A*, 169, 281
 Dickman, R. L., 1978, *ApJ*, 37, 407
 Dwarkadas, V. V., 2007, *ApJ*, 667, 226
 Frail, D. A., Goss, W. M., Reynoso, E. M., Giacani, E. B., Green, A. J., & Otrupcek, R. 1996, *AJ*, 111, 1651

Fazio, G. G., Hora, J. L., Allen, L. E., et al. 2004, *ApJS*, 154, 10
 Fich, M., Blitz, L., & Stark, A. A., 1989, *ApJ*, 342, 272
 Garden, R. P., Hayashi, M., Hasegawa, T., et al., 1991, *ApJ*, 374, 540
 Green, D. A., Frail, D. A., Goss, W. M., & Otrupcek, R. 1997, *AJ*, 114, 2058
 Hartmann, D., & Burton, W. B. 1997, *Atlas of Galactic Neutral Hydrogen* (Cambridge: Cambridge Univ. Press)
 Guesten, R., Serabyn, E., Kasemann, C., et al., 1993, *ApJ*, 402, 537
 Guetter, H. H. 1992, *AJ*, 103, 179
 Heiles, C., 1964, *ApJ*, 140, 470
 Hewitt, J. W., & Yusef-Zadeh, F. 2009, *ApJ*, 694, L16
 Huang, Y.-L., & Thaddeus, P. 1986, *ApJ*, 309, 804
 Jiang, B., Chen, Y., Wang, J. Z. et al., 2010, *ApJ*, 712, 1147
 Junkes, N., Fürst, E., & Reich, W., 1992, *A&A*, 261, 289
 Kharchenko, N. V., Piskunov, A. E., Röer, S., Schilbach, E., & Scholz, R.-D. 2005, *A&A*, 438, 1163
 Lang, K. R. 1980, *Astrophysical Formulae* (Berlin: Springer-Verlag), 157
 Leao, M. R. M., de Gouveia Dal Pino, E. M., et al., 2009, *MNRAS*, 394, 157
 Melioli, C., de Gouveia Dal Pino, E. M., et al., 2006, *MNRAS*, 373, 811
 Parons, S., Ortega, M. E., Rubio, M., & Dubner, G., 2009, *A&A*, 498, 445.
 Petriella, A., Paron, S., & Giacani, E., 2010, *A&A*, 513, A44
 Petriella, A., Paron, S., & Giacani, E., 2011, *Boletín de la Asociación Argentina de Astronomía*, 153, 221
 Reach, W. T., et al. 2006, *AJ*, 131, 1479
 Reynoso, E. M., & Mangum, J. G., 2001, *AJ*, 121, 347
 Riaz, B., Martín, E. L., Tata R., et al., 2012, *MNRAS*, 419, 1887
 Sanders, D. B., Scoville, N. Z., Tilanus, R. P. J., et al., 1993, in *Back to the Galaxy*, et. S. S. Holt & F. Verter (New York: AIP), 311
 Seta, M., et al. 1998, *ApJ*, 505, 286
 Sun, K., Ossenkopf, V., Kramer, C., et al., 2008, *A&A*, 489, 207
 Taylor, A. R., Wallace, B. J., & Goss, W. M., 1992, *AJ*, 103, 931
 Wilson, C. D., Walker, C. E., & Thornley, M. D., 1997, *ApJ*, 483, 210
 Wilner, D. J., Reynolds, S. P., & Moett, D. A. 1998, *AJ*, 115, 247
 Xu, J. L., & Wang, J. J., 2010, *RAA*, 2, 151
 Xu, J. L., Wang, J. J., & Miller, M., 2011a, *ApJ*, 721, 81
 Xu, J. L., Wang, J. J., & Miller, M., 2011b, *RAA*, 11, 537
 Xu, J. W., Zhang, X. Z., & Han, J. L., 2005, *Chin. J. Astron. Astrophys.*, 5, 165